Journal of Applied Electrochemistry **33**: 1077–1084, 2003.

Electrodeposition of antimony in a water-stable 1-ethyl-3-methylimidazolium chloride tetrafluoroborate room temperature ionic liquid

M-H. YANG and I-W. SUN*
Department of Chemistry, National Cheng-Kung University, Tainan, Taiwan, ROC 70101
*(*author for correspondence, e-mail: iwsun@mail.ncku.edu.tw)*

Received 17 December 2002; accepted in revised form 20 May 2003

Key words: antimony, electrodeposition, imidazolium chloride, ionic liquid, tetrafluoroborate

Abstract

The electrochemistry and electrodeposition of antimony were investigated on glassy carbon and nickel electrodes in a basic 1-ethyl-3-methylimidazolium chloride-tetrafluoroborate room temperature ionic liquid. Cyclic voltammetry results show that Sb(III) may be either oxidized to Sb(V) via a quasi-reversible charge-transfer process or reduced to Sb metal. Diffusion coefficients for both Sb(III) and Sb(V) species were calculated from rotating disc voltammetric data. Analysis of chronoamperometric current–time transients indicates that the electrodeposition of Sb on glassy carbon proceeded via progressive three-dimensional nucleation with diffusion-controlled growth of the nuclei. Raising the deposition temperature results in decreased average radius of the individual nuclei. Dense deposits can be obtained within a deposition temperature range between 30 to 120 °C. Scanning electron microscopy revealed dramatic changes in the surface morphology of antimony electrodeposits as a function of deposition temperature; deposits obtained at 30 °C had a nodular appearance whereas those obtained at 80 and 120 °C consisted of evenly distributed fine polygonal crystals.

1. Introduction

Room temperature ionic liquids [1–4] have attracted intensive interest in recent years as a replacement for classical molecular solvents in fundamental research and applications, including electrodeposition, batteries, catalysis, separations and organic synthesis. The advantages of these ionic liquids include good chemical and thermal stability, negligible vapour pressure, good electrical conductivity and a wide electrochemical window. The first group of ionic liquid systems that attracts attention is the chloroaluminates that are formed from dialkylimidazolium halides and aluminum halides [1]. Although the chloroaluminate ionic liquids have found many applications in electrodeposition [5], a major disadvantage of the chloroaluminate systems is that they are extremely reactive towards moisture and air so they must be handled under an inert atmosphere. Since 1992 [6, 7], various air- and moisture-stable ionic liquids have become available. The appearance of these water-stable ionic liquids has greatly accelerated research and applications using ionic liquids.

Antimony is a brittle silvery–white metal. Although the unalloyed form of antimony is not often used in industry, alloys of antimony have found wide commercial applications. The integration of antimony gives certain desirable properties, such as increased corrosion resistance, hardness, electrical resistivity and expansion on solidification [8, 9]. Moreover, antimony is also the component of some semiconductors such as InSb and $InAs_{1-x}Sb_x$. Thus, electrodeposition of antimony and its alloys is important from the viewpoint of its applications.

Although numerous examples of the electrodeposition of antimony from aqueous solutions can be found in the literature [8, 9], studies on the electrochemistry of antimony in ionic liquids are limited to the works of Osteryoung and coworkers [10, 11]. Their results show that Sb(III) can be reduced to Sb in the ionic liquids formed from aluminium chloride and *N*-butylpyridinium chloride ($AlCl_3$-BPC). However, these authors did not carry out deposition studies. In view of the advantages of the water-stable ionic liquids over the chloroaluminates and the fact that there have been few studies on electrodeposition in water-stable ionic liquids, we report here the electrochemistry of antimony(III) and the electrodeposition of antimony in a basic 1-ethyl-3-methylimidazolium chloride tetrafluoroborate (EMI–Cl–BF_4) room temperature water-stable ionic liquid containing an excess of free chloride ions. Previously we have reported electrochemical studies of copper and cadmium in the same ionic liquid system [12, 13]. Because one of the advantages of ionic liquids is that they can be used over a wide temperature range and because temperature can affect the deposition process significantly, the effects of deposition temperature on the

nucleation process and the morphologies of the electrodeposits are described.

2. Experimental details

2.1. *Apparatus*

All electrochemical experiments were conducted in a glove-box (Vacuum Atmosphere) filled with dry nitrogen. The moisture and oxygen contents in the box were kept lower than 1 ppm. The electrochemical experiments were accomplished by an EG&G PAR (model 273A) potentiostat controlled by EG&G PAR (model 270) software. A three-electrode cell was used. For voltammetry and chronoamperometry, the working electrode was either a glassy carbon rotating disc electrode (Pine Instrument Co., $A = 0.071$ cm^2) or a nickel electrode (BAS, $A = 0.071$ cm^2). The counter electrode was an aluminium (Aldrich, 99.99%) spiral immersed in pure ionic liquid contained in a glass tube having a fine porosity tip. The reference electrode was an aluminum wire immersed in a 60 mol % $AlCl_3$–EMIC melt contained in the same type of glass tube as the counter electrode. A Pine model AFMSR electrode rotator was employed for rotating disk electrode voltammetry. Electrodeposition experiments were conducted on nickel substrates (Aldrich 99.99%). A Hitachi S-4200 field effect scanning electron microscope (SEM) with an energy dispersive spectroscope (EDS) working at 15 kV was used to examine the surface morphology of the electrodeposits. The crystalline phases of the deposits were studied with a Shimadzu XD-D1 X-ray diffractometer.

2.2. *Chemicals*

1-Ethyl-3-methylimidazolium chloride was prepared and purified according to the literature [1]. Sodium tetrafluoroborate (Aldrich, 98%) and anhydrous $SbCl_3$ (Aldrich, 99.99%) were used as received. The EMI–Cl–BF_4 ionic liquid was prepared by direct reaction of appropriate amounts of EMIC and $NaBF_4$ in acetone as described previously [12]. Unless stated, the ionic liquid used in this study contains 0.11 M chloride ion, which was introduced by dissolution of EMIC. The density and the absolute viscosity of this ionic liquid at 30 °C were determined to be 1.248 g cm^{-3} and 0.358 g cm^{-1} s^{-1}, respectively.

3. Results and discussion

3.1. *Electrochemical behaviour of Sb(III)*

$SbCl_3$ dissolved readily in the EMI–Cl–BF_4 ionic liquid to form colourless solutions. It has been shown that in the basic (chloride-rich) $AlCl_3$–BPC ionic liquid, Sb(III) exists as $[SbCl_4]^-$ complex [10, 11], and this may also be

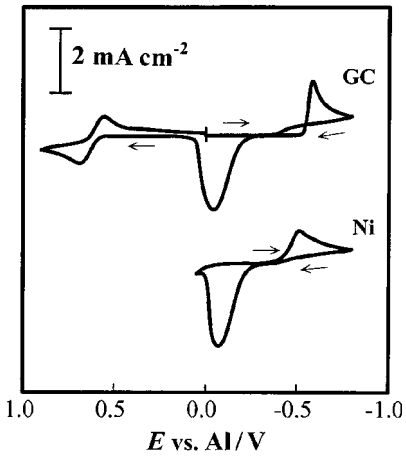

Fig. 1. Cyclic voltammograms recorded at a GC electrode and a nickel electrode for 10 mM Sb(III) in basic EMI–Cl–BF_4 ionic liquid at 30 °C. Sweep rate 100 mV s^{-1}.

true in the EMI–Cl–BF_4 ionic liquid. A typical cyclic voltammogram of $[SbCl_4]^-$ in the EMI–Cl–BF_4 ionic liquid at a glassy carbon electrode is shown in Figure 1. When the voltammetry was scanned in the positive direction and reversed at 0.90 V, an oxidation wave with a peak potential of about 0.68 V and a coupled reduction wave with a peak potential of about 0.56 V are apparent. To establish the oxidation state of the product of the oxidation of Sb(III), constant potential coulometry for the oxidation was conducted at 0.75 V. The total experimental charge consumed by the oxidation of 6.53×10^{-5} mol Sb(III) was 13.27 C, suggesting that the oxidation of Sb(III) is a two-electron process, that is, Sb(III) is oxidized to Sb(V). A Nernst plot was constructed for the Sb(III) and Sb(V) couple by adding different portions of $SbCl_3$ to adjust the concentration of Sb(III) while the concentration of the Sb(V) was kept constant in the solution. The equilibrium potentials, E_{eq}, were measured as a function of the [Sb(V)]/[Sb(III)] concentration ratio after each addition of $SbCl_3$. As shown in Figure 2, the resulting plot of E_{eq} vs ln[Sb(V)]/[Sb(III)] was linear with a slope of 12.9 mV. This experimental Nernst slope is in good agreement with

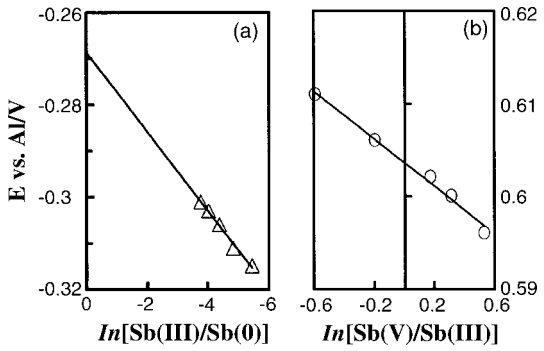

Fig. 2. Nernst plots for Sb(III)/Sb(0) and Sb(V)/Sb(III) redox couples in the basic EMI–Cl–BF_4 ionic liquid at 30 °C. Key: (△) Sb(III)/Sb(0); (○) Sb(V)/Sb(III). Solid lines: calculated from least-squares slopes and intercepts of electrochemical data.

Table 1. Cyclic voltammetric data for Sb(III)/Sb(V) in Basic EMI–Cl–BF_4 ionic liquid at a GC electrode at 30 °C

v /V s^{-1}	i_p^a /μA	$i_p^a v^{-1/2}$	E_p^c /V	E_p^a /V	$E_{p/2}$ /V	$(E_p^a - E_{p/2})$ /V
0.01	17.91	179	0.556	0.681	0.616	0.065
0.02	23.11	163	0.550	0.699	0.623	0.076
0.05	33.40	149	0.530	0.724	0.634	0.090
0.10	43.51	137	0.524	0.741	0.643	0.098
0.20	54.61	122	0.490	0.825	0.680	0.145

the theoretical slope, 13 mV, expected for a two-electron redox couple at 30 °C, indicating that the oxidation of Sb(III) indeed produces a Sb(V) species which is most likely to be $[SbCl_6]^-$ [11]. The intercept of the Nernst plot, which corresponds to the formal potential, $E^{\circ\prime}$, of the Sb(V)/Sb(III) couple is 0.60 V. In summary, this redox couple can be represented as follows:

$$[SbCl_4]^- + 2\,Cl^- \leftrightarrow [SbCl_6]^- + 2\,e^- \quad (1)$$

Data taken from the cyclic voltammograms for the oxidation of Sb(III) to Sb(V) are collected in Table 1. This table indicates that the anodic peak potential, E_p^a, for the oxidation of Sb(III) shifts positively with increasing potential scan rate, which is indicative of a slow charge-transfer reaction. Cyclic voltammograms of the Sb(V)/Sb(III) couple were also obtained on a GCRDE and a typical RDE voltammogram is shown in Figure 3. Plots of the GCRDE currents for the oxidation of Sb(III) against $\omega^{1/2}$ constructed from data taken at potentials on the ascending portion of the GCRDE voltammograms were not linear, indicating some kinetic complication. On the other hand, Figure 4 shows that plots of $1/i$ against $\omega^{-1/2}$ were linear in accordance with the equation [14]

$$1/i = 1/i_k + 1/i_{l,a} = 1/i_k + 1/(0.620nFACD^{2/3}v^{-1/6}\omega^{1/2}) \quad (2)$$

In Equation 2, $i_{l,a}$ is the limiting current for the oxidation of Sb(III), i_k is the current under pure kinetic control and all the other symbols have their usual meanings. Values for the potential dependent heterogeneous rate constant, $k_f(E)$, of this oxidation reaction are calculated from values of i_k determined from the intercepts of the plots of $1/i$ against $\omega^{-1/2}$ [14]:

$$i_k = nFAk_f(E)C \quad (3)$$

The standard heterogeneous rate constant, k° and the anodic transfer coefficient, α, were estimated from the slope and intercept of the ln $k_f(E)$ against E plot according to the following equation [14]:

$$\ln k_f(E) = \ln k^\circ - \alpha nFE/RT \quad (4)$$

The estimated values for k° and α are given in Table 2.

A set of the GCRDE voltammograms of the Sb(III)/Sb(V) couple showed that the limiting currents (i_l) against the square root of the rotation rate ($\omega^{1/2}$) were linear and passed through the origin for both the oxidation of Sb(III) and the reduction of Sb(V). The values of the limiting currents, obtained from the GC-RDE voltammograms, were used to calculate the diffusion coefficients, D, of the Sb(III) and Sb(V) species form the Levich equation. The results of these calculations along with the Stokes–Einstein products, $D\eta/T$, where η is the absolute

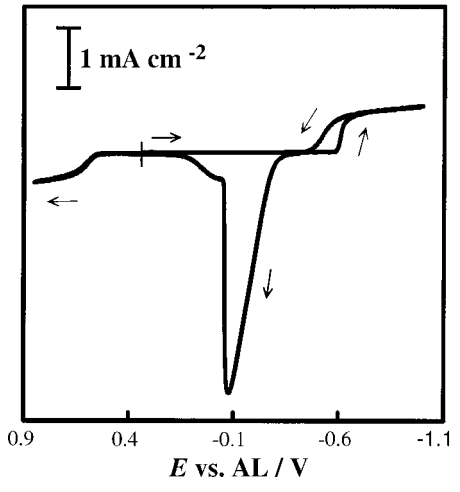

Fig. 3. GC rotating disc electrode voltammogram of 10 mM Sb(III) in basic EMI–Cl–BF_4 ionic liquid at 30 °C. Rotation rate 1000 rpm: potential sweep rate 5 mV s^{-1}.

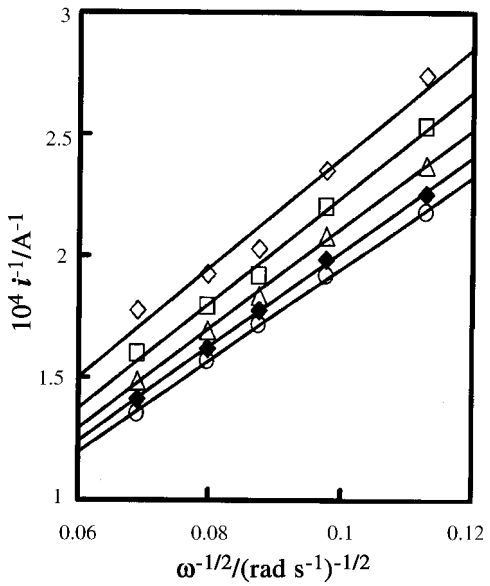

Fig. 4. Plots of reciprocal current against reciprocal square root of rotation rate for reduction of 10 mM Sb(III) in basic EMI–Cl–BF_4 ionic liquid at 30 °C. Key: (◇) −0.54, (□) −0.55, (△) −0.56, (◆) −0.57 and (○)−0.58 V.

Table 2. Summary of electrochemical data for Sb(III)/Sb(V) in basic EMI–Cl–BF_4 ionic liquid at 30 °C

Redox system	$E^{\circ\prime}$ /V	$10^7\ D$ /cm^2 s^{-1}	$10^{10}\ \eta DT^{-1}$ /g cm^2 s^{-2} K^{-1}	$10^5 k^\circ$/cm s^{-1}		α	
				W	GC	W	GC
Sb(III) → Sb(V)	0.60	2.98	3.49	9.8	6.2	0.37	0.22

viscosity of the ionic liquid, are collected in Table 2. This table indicates that the $D\eta/T$ values for both Sb(V) and Sb(III) species are comparable to the average value reported for '1−' charged anionic transition metal chloride complexes in basic $AlCl_3$–EMIC ionic liquid [15].

The cyclic voltammograms shown in Figure 1 indicate that when the potential was scanned negatively from the rest-potential, a cathodic peak arising from the reduction of Sb(III) to Sb and a coupled anodic peak due to the stripping of the deposited Sb are apparent. A negative shift in the cathodic peak potential with increasing scan rate indicates a slow charge-transfer reaction and/or an overpotential required nucleation. A hysteresis typical of that noted for nucleation overpotential deposition processes is observed on the reverse scan at the GC electrode but not at the Ni electrode, indicating that the nucleation of Sb at the GC substrate is kinetically less favored than at the Ni substrate. The integrated charge from the stripping peak equals the charge corresponding to the deposition peak, indicating that essentially all of the deposited Sb was recovered during oxidation. The equilibrium potential of the Sb(III)/Sb couple, E_{eq}, was estimated from the zero current intercepts of the reverse scans of the various cyclic GCRDE voltammograms [11]. The resulting E_{eq} values obtained with various Sb(III) concentrations were utilized to construct the Nernst plot for the Sb(III)/Sb couple. As shown in Figure 2, the resulting plot of E_{eq} against ln[Sb(III)]/[Sb(V)] was linear with a slope of 0.080 V. This experimental Nernst slope was in good agreement with the theoretical slope, 0.085 V, expected for a three-electron redox couple at 30 °C. The formal potential, $E^{\circ\prime}$, for the Sb(III)/Sb couple, determined from the intercept of the Nernst plot, was −0.27 V.

The effect of temperature on the cyclic voltammetric behaviour of electrodeposition of Sb on a GC electrode is illustrated in Figure 5. This Figure indicates that the deposition peak shifts positively with increasing temperature, suggesting that the electrodeposition of Sb at a higher temperature requires a smaller overpotential.

3.2. *Nucleation studies of the electrodeposition of Sb metal*

To further study the nucleation/growth process for the electrodeposition of Sb from Sb(III) at the GC electrode, chronoamperometry was performed at 30 °C, 80 °C, and 120 °C. These experiments were carried out by stepping the potential of the working electrode from a value where no reduction of Sb(III) would occur to potentials sufficiently negative to initiate a nucleation/growth process after a short induction time, t_o. A collection of the typical current–time transients from these chronoamperometry experiments is shown in Figure 6. The transients all exhibit the classical shape for a nucleation process, that is, after the decay of a sharp electrode double layer charging current, the faradaic current increases due to the nucleation and growth of Sb nuclei. This rising current eventually reaches a current maximum, i_m, as the discrete diffusion zones of each of the growing crystallites begin to overlap at time t_m. After time t_m, the current starts to decay due to the increase in diffusion layer thickness. The current–time transients in Figure 6 reveal that after t_m the transients converge to the experimental diffusion-limited Cottrell current at a longer time, indicating that the growth of Sb nuclei at GC electrode is diffusion limited.

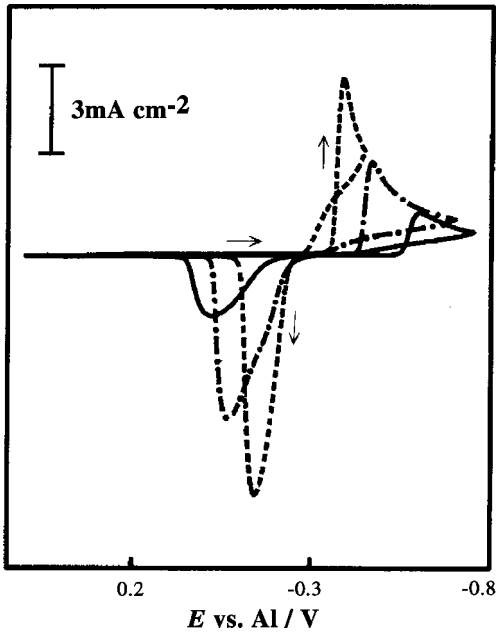

Fig. 5. Cyclic voltammograms of 10 mM Sb(III) in basic EMI–Cl–BF_4 ionic liquid recorded on GC electrode at (—) 30, (-·-·-) 80 and (- - -) 120 °C. Sweep rate 100 mV s^{-1}.

The experimental current-time transients can be expressed in normalized dimensionless forms to generate plots of $(i/i_m)^2$ against (t/t_m) [16]. These experimental plots are compared to the theoretical dimensionless current-transients derived for the three-dimensional 'instantaneous' and 'progressive' nucleation/growth models [16]. The experimental and theoretical plots are shown in Figure 7. It is apparent that, within the temperature range 30 °C to 120 °C, the electrodeposition of Sb at GC involves a three-dimensional progressive nucleation/growth process.

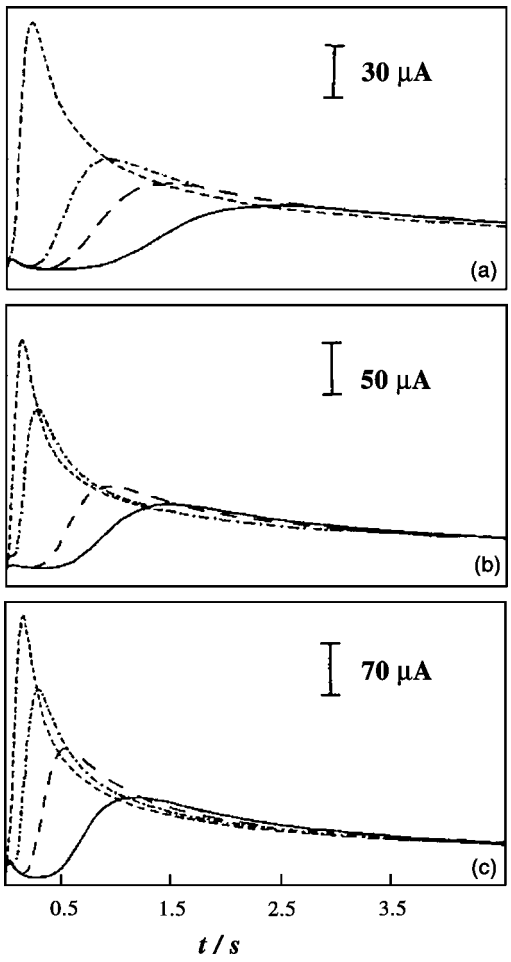

Fig. 6. Current–time transients resulting from chronoamperometry experiments recorded at a GC electrode for 10 mM Sb(III) in a basic EMI–Cl–BF_4 ionic liquid at (a) 30 °C: (—) −0.52, (– –) −0.54, (·····) −0.56 and (- - - -) −0.65 V; (b) 80 °C: (—) −0.41, (– –) −0.42, (·····) −0.45 and (- - - -) −0.50 V; (c) 120 °C: (—) −0.34, (– –) −0.36, (·····) −0.38 and (- - - -) −0.42 V.

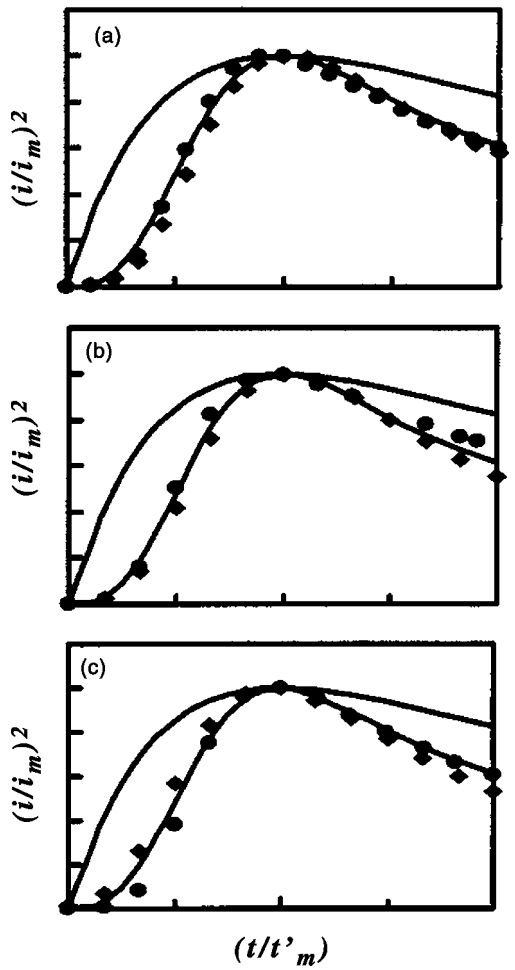

Fig. 7. Comparison of dimensionless experimental current–time transients derived from chronoamperometric experiments for 10 mM Sb(III) in basic EMI–Cl–BF_4 ionic liquid at a GC electrode with theoretical models for three-dimensional nucleation process. Temperature: (a) 30, (b) 80 and (c) 120 °C.

The three-dimensional progressive nucleation/growth process can be characterized by the product of the steady-state nucleation rate, $A(s^{-1})$, and the number density of active sites, N (cm^{-2}). This product can be calculated from the i_m of t'_m of the peak in the chronoamperograms, and the value of the saturation nuclear number density, N_s, as well as the average radius of the individual nuclei, r, can be estimated from the AN product [16]. The results of these calculations are plotted in Figure 8 as a function of the deposition overpotential, η. This figure shows that in the deposition overpotential range examined, N_s increases and r decreases as the overpotential increases. Figure 8 also shows that with the same deposition overpotential the saturation nuclear number density (N_s) increases with increasing deposition temperature.

3.3. *Bulk electrodeposition of antimony*

Bulk electrodeposits of Sb were prepared at thin nickel plates at different applied potentials at 30, 80, and 120 °C, respectively. Following each deposition experiment, the Sb-coated nickel plate was washed thoroughly with warm (~50 °C) deionized water to remove the residual ionic liquid. The ionic liquid was readily cleaned off the deposits because EMI–Cl–BF_4 ionic liquid is miscible with water and no side reactions that may damage the electrodeposits would occur during the washing. EDS analysis of the electrodeposit surfaces revealed that they were pure antimony with no trace of other elements such as Cl, B and F, indicating that no ionic liquid residue was trapped in the deposits. The XRD patterns recorded for several electrodeposits prepared at different temperatures are shown in Figure 9. In all cases, the deposits exhibit clear diffraction patterns that are consistent with pure antimony.

The surface morphology of bulk electrodeposits was examined by SEM and the resulting micrographs are illustrated in Figure 10. The deposit surface morphology changed dramatically as a function of the deposition temperature. Deposits prepared at 30 °C (Figure 10(a)) were dense rosette-like nodules. At higher magnification, these nodules seemed to be the agglomeration of embedded plates. Because the nucleation density

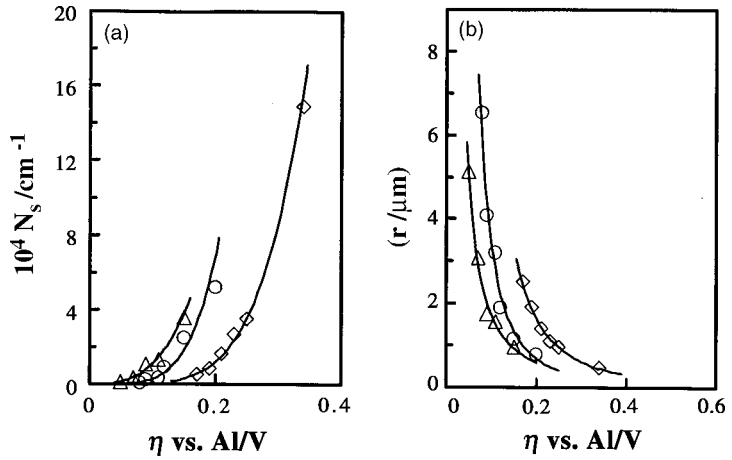

Fig. 8. Plots of (a) saturation nuclear number density, N_s, against overpotential, η and (b) average nucleus radius, r, against overpotential for the electrodeposition of Sb at GC electrode. Temperature: (◇) 30, (○) 80 and (△)120 °C.

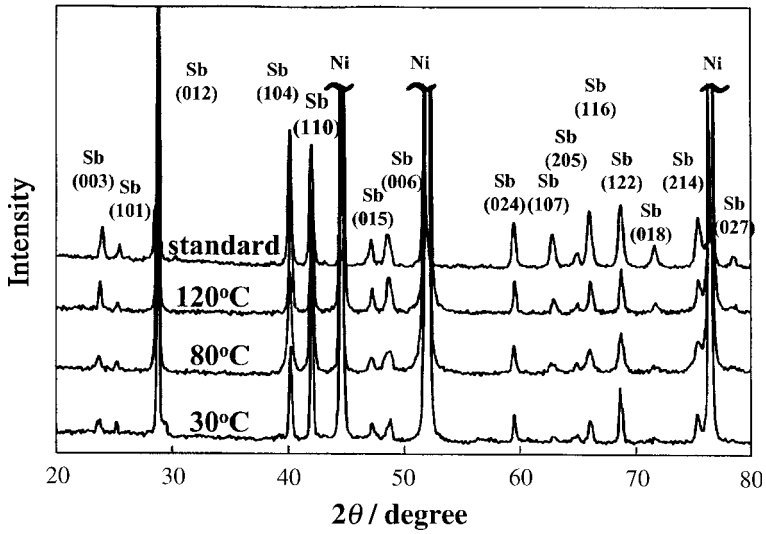

Fig. 9. XRD patterns (CuK_α) of standard Sb and Sb electrodeposits prepared at nickel substrates from Sb(III) in basic EMI–Cl–BF_4 ionic liquid at 30, 80 and 120 °C.

increases with increasing overpotential, the size of the nodules decreased as the deposition potential became more negative (Figure 10(b)), and eventually dendritic deposits were obtained at even more negative deposition potentials (not shown). Figure 10(c)–(f) show that when the deposition temperature was increased to 80 and 120 °C, the deposits lost their nodular structures and were more crystalline in appearance. As shown in these figures, the deposits obtained at 80 °C and 120 °C consisted of evenly distributed well-defined polygonal crystals. Figure 10(c) and (e) shows that at a more positive deposition potential with deposits dense and compact while Figure 10(d) shows a more negative deposition potential, resulting in a dendritic deposit at 80 °C. Figure 10(f) shows that at 120 °C the crystals became thinner when the deposition potential was made more negative. The deposits shown in Figure 10(c) and (e) have a bright metallic colour whereas those in Figure 10(d) and (f) are more or less grey. All the electrodeposits adhered well to the nickel substrate except the dendritic deposits that were formed at more negative deposition potentials.

4. Summary and conclusions

$SbCl_3$ dissolves readily in basic EMI–Cl–BF_4 ionic liquid. In this liquid, Sb(III) may be either oxidized to Sb(V) or reduced to Sb metal. The Sb(III)/Sb(V) reaction exhibits quasi-reversible charge-transfer behaviour at a glassy carbon electrode. The diffusion coefficients and Stoke–Einstein products calculated from rotating disc voltammetry data for both Sb(III) and Sb(V) are comparable to the average values reported for '1−' charged transition metal chloride complex anions. Chronoamprometry experiments revealed that the electrodeposition of Sb at a GC electrode proceeded via three-dimensional progressive nucleation with diffusion-

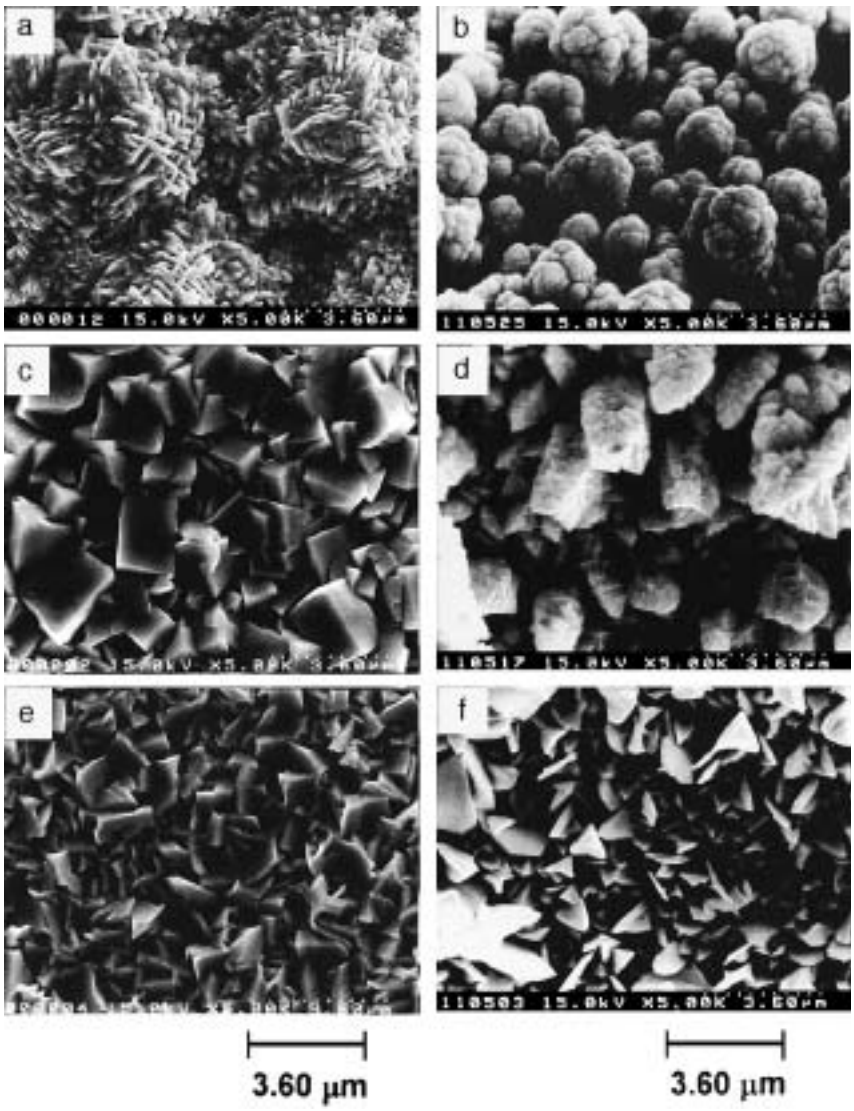

Fig. 10. SEM micrographs of antimony electrodeposited from Sb(III) in basic EMI–Cl–BF_4 ionic liquid at: (a), (b) 30 °C, (c), (d) 80 °C and (e), (f) 120 °C. Deposition overpotentials: (a) 0.05, (b) 0.23, (c) 0.10, (d) 0.11, (e) 0.10 and (f) 0.08 V.

controlled growth. Raising the deposition temperature increases the saturation nuclear number density and decreases the average radius of the individual nuclei, *r*. Bulk Sb electrodeposits were prepared on nickel substrates at 30, 80 and 120 °C. SEM showed that the deposition temperature has a significant effect on the surface morphologies of the deposits. Deposits prepared at 30 °C consisted of nodules which were not observed in deposits prepared at 80 and 120 °C. Instead, evenly distributed crystals were present in the compact and dense deposits obtained at 80 and 120 °C. The fact that good Sb electrodeposits could be obtained from the low temperature ionic liquids suggests that such liquids may be useful for the electrodeposition of Sb-containing materials such as InSb semiconductors.

Acknowledgement

This work was supported by the National Science Council of the Republic of China, Taiwan.

References

1. J.S. Wilkes, J.A. Levisky, R.A. Wilson and C.L. Hussey, *Inorg. Chem.* **21** (1982) 1263.
2. M.J. Earl and K.R. Seddon, *Pure Appl. Chem.* **72** (2000) 1391.
3. C.L. Hussey, *in* G. Mamantov and A.I. Popov (Eds), 'Chemistry of Nonaqueous Solutions Current Progress' (VCH, New York, 1994), p. 227.
4. R.T. Carlin and J.S. Wilkes, *in* G. Mamantov and A.I. Popov, *op. cit*. [3], p. 277.
5. G.R. Stafford and C.L. Hussey, *in* R.C. Alkire and D.M. Kolb (Eds), 'Advances in Electrochemical Science and Engineering', Vol. 7 (Wiley–VCH, 2001), p. 275.
6. J.S. Wilkes and M.J. Zaworotko, *J. Chem. Soc. Chem. Commum.* (1992) 965.
7. E.I. Cooper and E.J.M. O'Sullivan, *in* R.J. Gale, G. Blomgren and H. Kojima (Eds), 'Molten Salts' **PV 92-16** (Electrochemical Society Proceedings Series, Pennington, NJ, 1992), p. 386.
8. Y.N. Sadana, J.P. Singh and R. Kumar, *Surf. Technol.* **24** (1985) 319.
9. A. Brenner, 'Electrodeposition of Alloys, Principles and Practice' (Academic, New York, 1963).
10. D.A. Habboush and R.A. Osteryoung, *Inorg. Chem.* **23** (1984) 1726.
11. M. Lipsztjan and R.A. Osteryoung, *Inorg. Chem.* **24** (1985) 3492.

12. P-Y. Chen and I-W. Sun, *Electrochim. Acta* **45** (1999) 441.
13. P-Y. Chen and I-W. Sun, *Electrochim. Acta* **45** (2000) 3163.
14. A. Bard and L.R. Faulkner, 'Electrochemical Methods' (Wiley, New York, 1980).
15. C.L. Hussey, I-W. Sun, S.K.D. Strubinger and P.A. Barnard, *J. Electrochem. Soc.* **137** (1990) 2515.
16. T. Vargas and R. Varma, *in* R. Varma and J.R. Selman (Eds), 'Techniques for Characterization of Electrodes and Electrochemical Processes' (J. Wiley & Sons, New York, 1991), chapter 5.